Spectral Decomposition Method for Large Sea Surface Generation and Radar Backscatter Modeling

Article · November 2019

DOI: 10.1029/2018JC014070

Aymeric Mainvis
The French Aerospace Lab ONERA

Vincent Fabbro
The French Aerospace Lab ONERA

Bourlier Christophe
University of Nantes

Spectral Decomposition Method for Large Sea Surface Generation and Radar Backscatter Modeling

Aymeric Mainvis[1*], Vincent Fabbro[1], Christophe Bourlier[2], and Henri-Jose Mametsa[1]

[1]ONERA / DEMR, Université de Toulouse, F-31055 Toulouse - France
[2]IETR, Polytech Nantes, Nantes - France

Key Points:

- Fast and less-memory-demanding simulation of sea surface waves over a large area
- Quantitative analysis of the spectral decomposition method
- Study of the impact on the sea surface characteristics and on the radar backscatter

*2 avenue Edouard Belin, BP74025, 31055 Toulouse Cedex 4, France

Corresponding author: Aymeric Mainvis, `Aymeric.Mainvis@onera.fr`

This article has been accepted for publication and undergone full peer review but has not been through the copyediting, typesetting, pagination and proofreading process which may lead to differences between this version and the Version of Record. Please cite this article as doi: 10.1029/2018JC014070

Abstract

This paper analyzes different methods to simulate sea surface waves over a large area rapidly and with low computational complexity. Indeed, for wind speed between 1 and 10 m/s, the area of the sea surfaces must range from 10 to $92,000$ m^2 to account for all the surface roughness scales which can contribute to the scattering process at microwave frequencies. At frequencies higher than 10 GHz, a sampling rate of one-tenth of the wavelength can lead to a prohibitive numerical cost. The impact of these approaches on the surface power spectral density and on the monostatic normalized radar cross section (NRCS) is investigated. The proposed methods consist of splitting the full sea surface height spectrum into sub-spectra of smaller extents. Sub-sea surfaces are generated and combined from different interpolation and recombination techniques. In this paper, an original closed-form expression of the resulting sea surface height spectrum is derived to interpret the simulation results. Finally, the efficiency of the methods in terms of accuracy and memory requirement is analyzed by computing the monostatic NRCS from sea surfaces with the first-order Small Slope Approximation (SSA1) scattering model.

1 Introduction

Ocean observing systems –and remote sensing in particular– are an effective and efficient means to provide environmental data. The data can be useful for weather forecasting and climate change monitoring. One can use the data to conduct modeling to better understand and to make appropriate interpretations of the recorded data. More specifically, sea surface wave generation over a large area and with a high resolution is required in modeling some radar systems [*Franceschetti et al.*, 1998], [*Franceschetti et al.*, 2002], [*Ghaleb et al.*, 2010]. Indeed, building a realistic simulator of a real aperture radar (RAR) in a maritime environment implies the consideration of the spatial resolution of the system and correspondingly, the appropriate scale of the model of the sea surface waves, in order to be able to compute the electromagnetic wave scattering from this particular surface [*Ghaleb et al.*, 2010]. Therefore, it becomes crucial to have an efficient surface generation technique that does not involve lots of computational resources. Actually, modeling the electromagnetic (EM) wave scattering from realizations of random rough surfaces –using for example SSA1 [*Voronovich*, 1986]– needs a fine surface sampling grid to obtain accurate results. Commonly, this sampling grid size is chosen to be equal to one-tenth of the radar wavelength. Furthermore, a wide range of wavenumber is necessary to correctly represent the sea surface geometry. Therefore, EM scattering computations involving a large sea surface area entail increased computational cost and may rapidly become prohibitive.

The EM computations based on a "local-interaction only" approach like a Kirchhoff-type integral (such as SSA1) at a single frequency, demand only one numerical integration per observation direction. Therewith, the computational cost is dominated by the generation of the sea surface. Realizations of the sea wave height profile are created from a centered reduced Gaussian process multiplied by the square root of the power spectral density in the Fourier domain. The required memory for such a method, with the Fast Fourier Transform (FFT), can exceed the available memory for large scenes. A fast and memory cheap simulation of a sea surface has been described in [*Pinel et al.*, 2014][*Jiang et al.*, 2015]. Pinel et al. studied the slope probability density function and the slope autocorrelation function after dividing the spectrum of the sea height profile into two parts and generating sea surfaces with different spatial resolutions and different spatial areas. In [*Jiang et al.*, 2015], a Spectral Decomposition Method (SDM) has been introduce to reduce the memory requirements and to generate different-scale rough surfaces. In the SDM, the complete height spectrum is divided into several parts, each one used to generate a specific surface roughness. This method is particularly well-suited to perform unified device architecture (CUDA) parallel computation. The same method has been studied for sea surface wave generation in [*Jiang et al.*, 2016] and tested with SSA1 by simulating the sea surface NRCS and Doppler spectra. The Doppler spectrum of the sea surface has also been studied in [*Wei et al.*, 2018].

In this paper, the computational cost of the SDM approach and the conventional one –which corresponds to the spectral method for sea surface realizations which is extensively described in [*Tessendorf*, 2001]– are compared and the monostatic normalized radar cross section (NRCS) is computed with SSA1. The first originality of this paper is to provide a quantitative analysis of the spectral decomposition method. Truly, this particular sea surface generation is analytically described and developed to express its computational complexity. Secondly, a study is performed to highlight the impact of both the interpolation process (to overcome spatial resolution issues) and the two suggested combination techniques (to solve the large spatial extent issue) on the sea surface geometry characteristics and on the monostatic NRCS. The latter is computed by using the SSA1 introduced by Voronovich et al. [*Voronovich*, 1986]. Arguably, this model is relevant due to an easy-to-use expression and it provides accurate results. Indeed, regarding more complex models like the full SSA, the SSA1 model can predict the NRCS with a precision of 1 and 2 dB for the VV and HH polarizations, respectively [*Voronovich and Zavorotny*, 2001], [*McDaniel*, 2001], [*Bourlier and Pinel*, 2009], [*Bourlier*, 2018]. However, the spectral decomposition method remains applicable for more complex scattering methods anyways.

This paper is organized as follows. Section 2 details the formalism of the SDM which describes a split-spectrum process and a reconstructed sea surface generation with an interpolated surface and a combination technique. The computational complexity and the memory consumption of the SDM are also made explicit. Section 3 presents the SSA1 method, the sea surface NRCS expression and the link between the sea surface parameters and the electromagnetic scattering characteristics. Section 4 presents numerical results for a two-dimensional problem by evaluating the sea surface height spectrum and the height structure function. The monostatic NRCS computed with the SSA1 method considering a conventional sea surface generation and the SDM are described before discussing the influence of the SDM parameters in Section 5.

2 Sea Surface Generation and Spectral Decomposition Method

This section provides the theoretical materials of the paper. It develops the sea surface model, the formalism of the spectral decomposition method and the sea surface generation with an interpolated surface and a combination technique. Also, the significance of the spectral decomposition method is highlighted by explicit figures for the computational complexity and the memory consumption.

2.1 Sea Surface Model

The height of the sea surface $H(\mathbf{r}, t)$ is conventionally given in spectral form (see [*Tsang et al.*, 2002]). The generic expression is

$$H(\mathbf{r}, t) = \mathrm{Re}\left[\int_{\mathbb{R}^2} \sqrt{S(\mathbf{k})} E(\mathbf{k}) e^{-j\omega(\mathbf{k})t} e^{j\mathbf{k}\cdot\mathbf{r}} d\mathbf{k}\right], \tag{1}$$

where $\mathbf{r} = (x, y)$ are the Cartesian position coordinates, t the time, $S(\mathbf{k})$ the sea height spectrum, $\mathbf{k}$ the wavenumber vector, E a Gaussian process –with zero-mean and unit standard deviation– and $\omega(\mathbf{k})$ the pulsation defined by means of a dispersion relation [*Elfouhaily et al.*, 1997]. This conventional expression can be very efficiently computed with the Fast Fourier Transform (FFT). However, EM scattering computation using rigorous techniques requires a fine sampling of the surface and this may lead to prohibitive computing resources at high frequency and for high sea states in a three-dimensional problem. For this reason an optimization of the method is proposed by applying a decomposition of the spectrum.

2.2 Spectral Decomposition Method

To optimize memory requirements and computation times of sea surface wave generation, the general idea is to decompose the surface into sub-surfaces in the spectral domain. To introduce the spectral decomposition method; first, function Γ is defined by

$$\Gamma(\mathbf{k},t) = \sqrt{S(\mathbf{k})}E(\mathbf{k})e^{-j\omega(\mathbf{k})t}. \tag{2}$$

Then, this function is decomposed as a sum of N functions Γ_n defined by

$$\Gamma_n(\mathbf{k},t) = \begin{cases} \Gamma(\mathbf{k},t) & \text{if } k_n \leq \|\mathbf{k}\| < k_{n+1} \\ 0 & \text{otherwise,} \end{cases} \tag{3}$$

with Γ defined in (2), $\|\cdot\|$ the norm of a vector, $\mathbf{k}$ the wavenumber vector, k_n the cutoff-wavenumber, for which $k_0 = 0$, $k_N = +\infty$ and $n \in [0, N-1]$. Consequently, one has to choose $N-1$ cutoff-wavenumbers k_n to define Γ_n. Eq. (1) can then be rewritten as

$$\begin{aligned} H(\mathbf{r},t) &= \mathrm{Re}\left[\sum_{n=0}^{N-1}\int_{\|\mathbf{k}\|=k_n}^{\|\mathbf{k}\|=k_{n+1}} \Gamma(\mathbf{k},t)e^{j\mathbf{k}\cdot\mathbf{r}}d\mathbf{k}\right] \\ &= \mathrm{Re}\left[\sum_{n=0}^{N-1}\int_{\mathbb{R}^2} \Gamma_n(\mathbf{k},t)e^{j\mathbf{k}\cdot\mathbf{r}}d\mathbf{k}\right] \\ &= \sum_{n=0}^{N-1} h_n(\mathbf{r},t), \end{aligned} \tag{4}$$

with $h_n(\mathbf{r},t)$ the height of the sea surface generated from the n-th spectral constituent Γ_n. The full sea surface $H(\mathbf{r},t)$ is obtained by summation of all N constituent sea surfaces corresponding to the various roughness ranges.

2.3 Reconstructed Sea Surface

Geometry Definition

To illustrate the splitting-up process introduced in (3), an example is presented here. The sea height spectrum in (1) is divided into two sub-spectra S_0 and S_1 derived from the function Γ_n in (3). These sub-spectra lead to the realization of two elementary sea surfaces h_0 and h_1 (4).

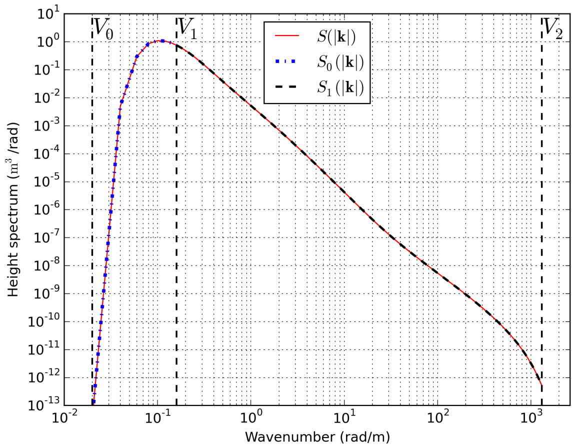

Figure 1: Isotropic part of the sea surface height spectrum S. The spectrum S is split up into two sub-spectra S_0 and S_1 using the model of Elfouhaily et al. [*Elfouhaily et al.*, 1997]. Wind speed is $u_{10} = 8$ m/s.

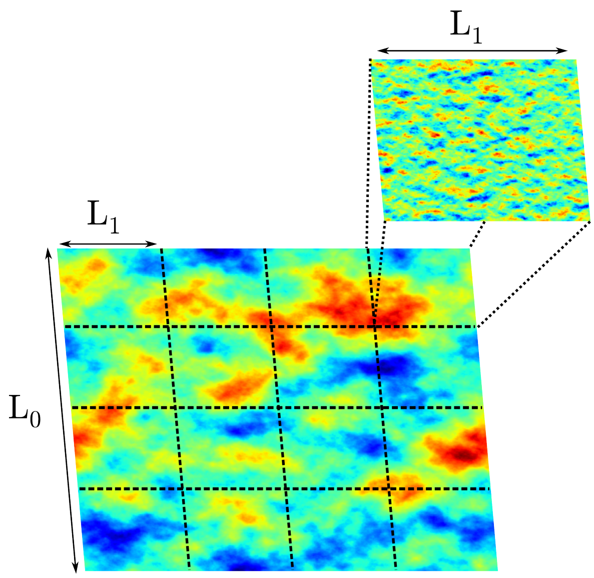

Figure 2: Realization of the two elementary sea surfaces h_0 and h_1

Figure 1 plots an example of the splitting-up process to generate two elementary sea surfaces h_0 and h_1 (Figure 2) from the two sub-spectra S_0 and S_1 defined on $[V_0, V_1]$ and $[V_1, V_2]$ respectively. Here, by using the FFT, the wavenumber V_0 fixes the length L_0 of the first sea surface h_0, $V_1 = \pi/\Delta X_0$ is the chosen cutoff-wavenumber linked to the length L_1 of the second sea surface h_1 and to the spatial sampling interval of h_0 marked ΔX_0. At last, $V_2 = \pi/\Delta X$ fixes the spatial sampling interval of the second sea surface h_1 marked ΔX. To sum up, two elementary sea surfaces h_0 and h_1 are generated with two different lengths and two different spatial sampling intervals which are $(L_0, \Delta X_0)$ for h_0 and $(L_1, \Delta X)$ for h_1. They correspond to the low and high parts of the sea spectrum plotted in Figure 1.

In the general case, computing sea surface implies choosing a surface size $L_x \times L_y$ (or $M_x \times M_y$ sampling points) and sampling intervals (Δ_x, Δ_y). For more clarity, in this paper, the surface length and the sampling interval to generate the sea surface H are chosen such that $L_x = L_y = L_0$ and $\Delta_x = \Delta_y = \Delta X$, respectively. Then, SDM in its practical form –that is in discretized form– consists in generating the N constituent sea surfaces defined by the N functions Γ_n in (3) via FFT. Considering the discretization problem along only one axis (to lighten the expressions), the discretized wavenumbers of the n-th function Γ_n are $K_{m,n} = m\Delta K_n$ with $m \in [-M_n/2, M_n/2]$ and $n \in [0, N-1]$, M_n sampling points and $\Delta K_n = 2\pi/L_n$ the step in the spectral domain dictating the n-th surface length $L_n = M_n \times \Delta X_n$, ΔX_n being the spatial sampling interval of the n-th elementary generated sea surface. Here, $\Delta K_0 = 2\pi/L_0$, the other steps in the spectral domain are freely selected and correspond to the cutoff-wavenumbers k_n, $n \in [1, N-1]$ in (4). Moreover, the spatial sampling interval ΔX is the one of the N-th elementary generated sea surface, $\Delta X_{N-1} = \Delta X$. So, by considering N interlocked sub-surfaces, selecting the cutoff-wavenumbers in SDM leads to the parameters of h_n in (4)

$$L_n = \frac{2\pi}{\Delta K_n} \qquad \Delta X_n = \frac{2\pi}{M_n \Delta K_n}, \tag{5}$$

with ΔK_n the step in the spectral domain and ΔX_n the sampling interval in the spatial domain. In this paper, $M_n = M$ is a constant, this implies

$$L_n > L_{n+1}, \tag{6}$$

and, therewith

$$\Delta X_n > \Delta X_{n+1}. \tag{7}$$

Consequently, the heart of SDM consists of generating a series of sea surfaces, each one with a particular height function over a chosen area and with its appropriate sampling interval or mesh.

However, to be able to superpose the different surfaces corresponding to the different roughness scales, the surface meshes must be equal. To solve this problem, two techniques are investigated: an interpolation process and a combination technique. Figure 3 plots a schematic diagram for the generation of surfaces h_n and h_{n+1} and their respective length, L_n and L_{n+1}, and sampling interval, ΔX_n and ΔX_{n+1} according to the SDM.

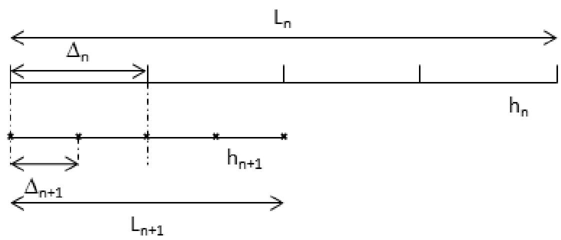

Figure 3: Schematic diagram for the generation of surfaces h_n and h_{n+1} according to the Spectral Decomposition Method.

The interpolation process serves to reduce the sampling interval from ΔX_n to ΔX, the smallest sampling interval. In this paper, three kinds of interpolation are studied, namely, linear, quadratic and cubic. The combination technique serves to extend a surface height profile computed over a length L_n to a profile over the full length L_0. The interpolation and combination methods are applied hierarchically. Figure 3 shows the interpolation and combination steps between two levels of the hierarchy. For the sake of clarity, we elaborate a two-dimensional problem and a spectrum partitioned into only two parts (see Figure 1). Therefore, the total sea surface H is composed of a low-frequencies-scale (LF) constituent h_{LF} and a high-frequencies-scale (HF) constituent $h_{\mathrm{HF,T}}$

$$H(x) = h_{\mathrm{LF}}(x) + h_{\mathrm{HF,T}}(x), \tag{8}$$

h_{LF} is the interpolated sea surface and $h_{\mathrm{HF,T}}$ the combined one.

Combination Technique Expressions

Two combination techniques are studied: the Repeated Surfaces Technique (RST) and the Combined Surfaces Technique (CST). The RST principle is that the final HF surface is composed of A times the same realization of the elementary HF surface (this approach is thus directly applicable for a three-dimensional problem). It can be formalized by

$$h_{\mathrm{HF,T}}(x) = h_{\mathrm{HF}}(x) * \sum_{a=0}^{A-1} \delta(x - aL), \tag{9}$$

with $*$ the convolution product, h_{HF} the elementary HF surface, L its length, $h_{\mathrm{HF,T}}$ the composed surface of length AL and δ the Dirac distribution. This combination technique ensures the continuity of the combined surface h_{HF} due to the periodicity properties of the FFT. Considering a three-dimensional problem, Jeannin et al. [*Jeannin et al.*, 2012] proposed the CST approach. Unlike the RST, this approach is well-suited to a random process because it preserves the statistical features of the elementary random surface, such as the correlation, the mean value and the variance. With a CST adapted to a two-dimensional problem, the composite surface h_{comp} is defined by

$$h_{\mathrm{comp}}(x) = \frac{\sqrt{d-x}\, z_1(x + L - d) + \sqrt{x}\, z_2(x)}{\sqrt{d}}, \tag{10}$$

with $x \in [0; d]$, z_1 and z_2 two independent rough surfaces with length L. These two surfaces are to be combined on an interval d. Then,

$$h_{\mathrm{HF,T}}(x) = \sum_{a=0}^{A-1} h_{\mathrm{HF,int},a}(x) * \delta[x - a(L-d)], \tag{11}$$

with

$$h_{\mathrm{HF,int},a}(x) = \begin{cases} h_{\mathrm{HF,comp},a-1}(x) & \text{if } x \in [0; d] \\ h_{\mathrm{HF},a}(x) & \text{if } x \in]d; L-d], \end{cases} \tag{12}$$

$h_{\mathrm{HF},a}$ the a-th realization of the elementary HF surface with a length L and

$$h_{\mathrm{HF,comp},a}(x) = \frac{\sqrt{d-x}\, h_{\mathrm{HF},a}(x + L - d) + \sqrt{x}\, h_{\mathrm{HF},a+1}(x)}{\sqrt{d}}. \tag{13}$$

Thus $h_{\mathrm{HF,int},a}$ is a rough surface of length $(L-d)$. Furthermore,

$$h_{\mathrm{HF,comp},-1}(x) = \frac{\sqrt{d-x}\, h_{\mathrm{HF},A-1}(x + L - d) + \sqrt{x}\, h_{\mathrm{HF},0}(x)}{\sqrt{d}}, \tag{14}$$

to ensure the continuity of the combined sea surface. The length of the composed surface $h_{\mathrm{HF,T}}$ is equal to $(L-d)A$. For simplicity, the interval d is taken to be $L/2$ in this work. Figure 4 illustrates a schematic diagram for the generation of the surface $h_{\mathrm{HF,T}}$ with each of the two combination techniques, RST Figure 4a and CST Figure 4b.

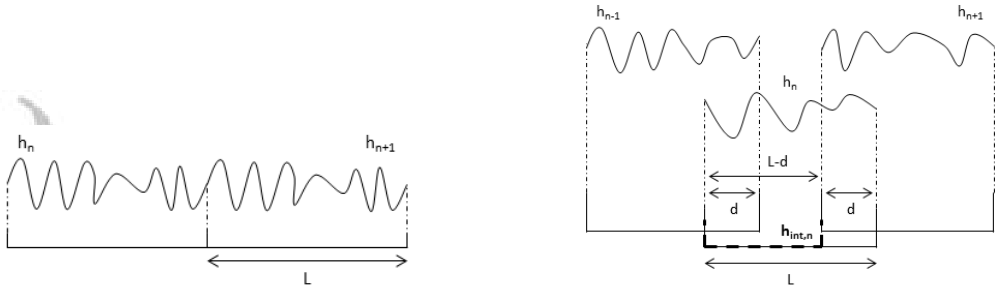

(a) Repeated Surfaces Technique (b) Combined Surfaces Technique

Figure 4: Schematic diagram for the generation of the combined surface $h_{\mathrm{HF,T}}$ with each of the two combination techniques, RST (4a) and CST (4b).

To check the sea spectrum integrity, the HF sea height spectrum from RST is expressed, that is the spectrum derived from (9). It can be written as

$$S_{\mathrm{HF,RST}}(k) = \frac{S_{\mathrm{HF}}(k)}{A} \frac{\sin^2\left(\frac{kAL}{2}\right)}{\sin^2\left(\frac{kL}{2}\right)} \tag{15}$$

with $S_{\mathrm{HF,RST}}$ the RST spectrum, S_{HF} the sea height spectrum used to generate the A combined surfaces of length L and k is the wavenumber. The proof is detailed in Appendix A. Then, from (15), it appears that $S_{\mathrm{HF,RST}}$ is the conventional sea spectrum S_{HF} modulated by a $2\pi/L$-periodic function. This function has local maxima for

$$\frac{kL}{2} = n\pi \Leftrightarrow k = \frac{n2\pi}{L}, \tag{16}$$

with $n \in \mathbb{Z}$.

2.4 Computational Complexity and Memory Space

To quantify the efficiency of the SDM, the computational complexity of the FFT is a relevant tool. This is expressed as

$$\mathcal{O}(s_T \log_2 s_T), \tag{17}$$

with s_T the number of samples used in the FFT. Let us consider a simple 3D case, as previously discussed, the spectrum is divided into two parts like in (8), that is

$$H(\mathbf{r}, t) = h_{\mathrm{LF}}(\mathbf{r}, t) + h_{\mathrm{HF,T}}(\mathbf{r}, t), \tag{18}$$

where h_{LF} is the interpolated sea surface and $h_{\mathrm{HF,T}}$ the reconstructed one. According to the chosen combination technique, the computational complexity $C_{\mathrm{HF,T}}$ of the surface generation $h_{\mathrm{HF,T}}$ is

$$C_{\mathrm{HF,T}} = \begin{cases} \mathcal{O}(s_{\mathrm{HF}}^2 \log_2 s_{\mathrm{HF}}^2) & \text{if RST} \\ \frac{L^2}{(L-d)^2} P^2 \times \mathcal{O}(s_{\mathrm{HF}}^2 \log_2 s_{\mathrm{HF}}^2) & \text{if CST,} \end{cases} \tag{19}$$

with s_{HF}^2 the number of samples of each elementary combined surface of area L^2, d the CST parameter in (11) and P such as $P{\times}L = L_0$ with L_0^2 the area of the total surface H. The computational complexity of the interpolation process can be considered negligible with regard to the one of the FFT. In particular, the computational complexity of linear interpolation is one multiplication and two additions per sample of output. So, the computational complexity C_H to generate the sea surface H is

$$C_H = \mathcal{O}(s_{\mathrm{LF}}^2 \log_2 s_{\mathrm{LF}}^2) + C_{\mathrm{HF,T}}, \tag{20}$$

with s_{LF}^2 the number of samples of the low-frequencies-scale sea surface before interpolation. For example, suppose $s_{\mathrm{LF}} = s_{\mathrm{HF}} = s$, then,

$$C_H = (1+\alpha) \times \mathcal{O}(s^2 \log_2 s^2), \tag{21}$$

$\alpha = 1$ (RST) or $P^2L^2/(L-d)^2$ (CST) from (19). However, one of the most interesting aspects of the SDM is that the overall generated sea surface does not need to be stored to perform the EM wave scattering calculations because of the additivity of the integral over the intervals. The actual parameter α remains 1 for RST but becomes only 4 for CST. Indeed, during the EM wave scattering estimation, only $h_{\mathrm{HF,int},a}$ from (11) has to be stored, this surface needs 4 elementary HF surfaces in a three-dimensional problem. The equivalent computational complexity C_{ref} for a conventional sea surface generation is

$$C_{\mathrm{ref}} = \mathcal{O}(P^2 s^2 \log_2 P^2 s^2). \tag{22}$$

Indeed, with a given number of samples s^2 and a given sampling interval ΔX, the total area of the generated sea surface with SDM is $L^2 = (P \times s \times \Delta X)^2$. So, by keeping the same sampling interval, $(s \times P)^2$ sampling points are needed to reach the same area with a conventional approach.

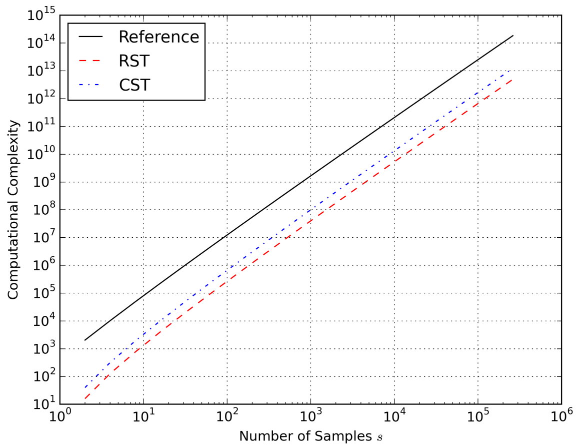

Figure 5: Computational complexity of sea surface generation versus the number of samples s with $P = 8$

Figure 5 sets out the computational complexity of sea surface generation versus the number of samples s with $P = 8$ according to (21) (RST and CST) and (22) (Reference). For a number of samples $s = 10^4$, this result shows a gain between 12 and 14 by using SDM rather than a conventional sea surface generation. Figure 6 plots the computational complexity of sea surface generation versus the parameter P –defined in (19)– with $s = 2^{13}$. This time, the gain is between 160 (for CST) and 200 (for RST) when using SDM with $P = 16$. These simulations clearly highlight the benefits of such a multiscale method.

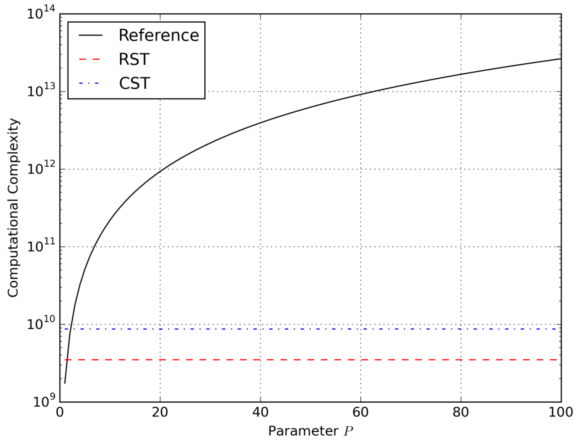

Figure 6: Computational complexity of sea surface generation versus the parameter P with $s = 2^{13}$

As to memory requirements, by keeping the same notations introduced in (21) and (22), the total memory space needed to store generated sea surface data is

$$\begin{aligned} M_{\mathrm{ref}} &= mP^2 s^2 \quad (23) \\ M_H &= m(1+\alpha)s^2, \quad (24) \end{aligned}$$

where m is the memory allocated for an elementary piece of data, M_{ref} the memory needed for a conventional sea surface generation and M_H the the memory required with the SDM, with $\alpha = 1$ or 4 using RST or CST, respectively. According to Elfouhaily et al. [*Elfouhaily et al.*, 1997],[*Bourlier et al.*, 2013], the minimum surface wavenumber $k_{\min}$ should verify $k_{\min} \approx 0.3 k_p$ with

$$k_p \approx \Omega^2 g / u_{10}^2, \quad (25)$$

where Ω is the inverse wave age equal to 0.84 in the case of a fully developed sea, g the acceleration of gravity and u_{10} the wind speed at ten meters above the sea. So, with a sampling interval of one-tenth of the incident radar wavelength –considering a radar frequency of 10 GHz– and $u_{10} = 8$ m/s; $4,175,199,906$ samples are needed to generate a conventional 3D sea surface. That is $2^{35} = 34,359,738,368$ bytes for a *float64* ($m = 8$ bytes) which is hardly restrictive in terms of computational resources (34 GB of RAM, random access memory, is thus necessary) or about time consumption (to extend RAM by reading and writing on flash memory). Furthermore, these values are linked to $u_{10} = 8$ m/s corresponding to a sea state of 4 over 9 in a case of a fully developed sea. Then, the higher the sea state is, the more computational resources are needed. For SDM, with $\alpha = 1$ for RST and $P = 8$ combined surfaces, $M_H = 1,043,799,976$ bytes. The memory consumption ratio is 1/32. Table. 1 gives the memory consumption ratio M_H / M_{ref} versus the parameter P and the combination technique. Once again, the SDM is more efficient than the conventional sea surface generation and so, more sea states can be considered for a limited memory space.

Table 1: Memory Consumption Ratio

Parameter P	RST	CST
$P = 8$	0.031	0.078
$P = 16$	0.008	0.020
$P = 32$	0.002	0.005

In this section, it has been shown that the SDM is efficient for simulating a sea surface. The main objective of this paper is to efficiently compute the radar backscattering of an ocean surface. In order to assess the benefits of the SDM, its performance in a radar backscatter modeling needs to be studied too. This is the subject of the next section.

3 Simulated Radar Backscattering: First-Order Small Slope Approximation

This section discusses the mathematical and physical links between the sea surface parameters and the electromagnetic scattering properties. It emphasizes the surface-specific parameters –driven by the SDM– that are crucial for the NRCS estimation. The NRCS is computed by a local model, the first-order Small Slope Approximation (SSA1) which is accurate in the whole range of incidence angles, from 0° (nadir) to 60°. The scattering operator is given by [*Voronovich*, 1986]

$$\mathbb{S}(\mathbf{k_s}, \mathbf{k_0}) = \frac{2(q_s q_0)^{1/2}\mathbb{B}(\mathbf{k_s}, \mathbf{k_0})}{Q_z} \int_{\mathbf{r}} e^{-jQ_z\eta(\mathbf{r})} e^{-j\mathbf{Q_H}\cdot\mathbf{r}} d\mathbf{r}, \tag{26}$$

where $\mathbb{B}(\mathbf{k_s}, \mathbf{k_0})$ is the first-order small perturbation model (SPM1) kernel [*Voronovich and Zavorotny*, 2001], a polarization term. $\mathbf{Q_H}$ and Q_z are the horizontal and vertical components of the vector $\mathbf{Q} = \mathbf{k_s} - \mathbf{k_0}$, respectively. $\mathbf{k_0}$ (with $-q_0$ the vertical component) and $\mathbf{k_s}$ (with $+q_s$ the vertical component) are the incidence and observation wave vectors, respectively and $\eta(\mathbf{r})$ is the surface elevation. In its computed form, the generated sea surface geometry induces a limited integration area in (26) and it leads to the modified scattering operator

$$\mathbb{S}_{\mathrm{mo}}(\mathbf{k_s}, \mathbf{k_0}) = \frac{2(q_s q_0)^{1/2}\mathbb{B}(\mathbf{k_s}, \mathbf{k_0})}{Q_z} \int_{\Sigma} e^{-jQ_z\eta(\mathbf{r})} e^{-j\mathbf{Q_H}\cdot\mathbf{r}} d\mathbf{r}, \tag{27}$$

with Σ the effective illuminated area (length in a 2D problem). Then, the incoherent NRCS of a finite surface σ_0 is expressed as

$$\sigma_0(\mathbf{k_s}, \mathbf{k_0}) = \frac{\langle \mathbb{S}_{\mathrm{mo}}(\mathbf{k_s}, \mathbf{k_0})\mathbb{S}^*_{\mathrm{mo}}(\mathbf{k_s}, \mathbf{k_0})\rangle}{\kappa\Sigma} - \frac{\langle \mathbb{S}_{\mathrm{mo}}(\mathbf{k_s}, \mathbf{k_0})\rangle\langle \mathbb{S}_{\mathrm{mo}}(\mathbf{k_s}, \mathbf{k_0})\rangle^*}{\kappa\Sigma}, \tag{28}$$

with $\mathbb{S}_{\mathrm{mo}}(\mathbf{k_s}, \mathbf{k_0})$ defined in (27) and κ a constant equal to π for a 3D problem and $4k_0$ for a 2D problem with k_0 the radar wavenumber. In this numerical approach, a Thorsos beam [*Bourlier et al.*, 2013] of parameter $g = L/3$ (with L the total length of the sea surface) is considered to illuminate the generated sea surface. This beam is a tapered plane wave with a Gaussian shape. The tapering is used to reduce the incident field to near zero at the edges of the generated sea surface waves and so, to reduce the potential edge effects to a negligible level. From (28) and for a Gaussian process, an analytical expression of the incoherent NRCS [*Bourlier et al.*, 2005] can also be derived,

$$\begin{aligned} \sigma_0(\mathbf{k_s}, \mathbf{k_0}) &= \frac{4q_s q_0 \left|\mathbb{B}(\mathbf{k_s}, \mathbf{k_0})\right|^2}{\kappa Q_z^2} e^{-Q_z^2\sigma_\eta^2} \int_{\Sigma} e^{-j\mathbf{Q_H}\cdot\mathbf{r}} \left[e^{Q_z^2 W(\mathbf{r})} - 1\right] d\mathbf{r} \\ &= \frac{4q_s q_0 \left|\mathbb{B}(\mathbf{k_s}, \mathbf{k_0})\right|^2}{\kappa Q_z^2} \int_{\Sigma} e^{-j\mathbf{Q_H}\cdot\mathbf{r}} \left[e^{-\frac{1}{2}Q_z^2\mathcal{D}(\mathbf{r})} - e^{-Q_z^2\sigma_\eta^2}\right] d\mathbf{r}, \end{aligned} \tag{29}$$

with σ_η^2 the mean square value of the height, W the autocorrelation function of the height and $\mathcal{D}$ the height structure function defined as

$$\mathcal{D}(\mathbf{r}) = 2\left[\sigma_\eta^2 - W(\mathbf{r})\right]. \tag{30}$$

The analytical expression in (29) is the easiest way to calculate the theoretical NRCS from an infinite sea surface. But, as previously mentioned, in realistic simulators, the spatial resolution of the radar has to be taken into account and this requires a set of sea surface realizations and compute the average values in (28). Furthermore, in (29), the monostatic NRCS ($\mathbf{k_s} = -\mathbf{k_0}$) is directly linked to the Fourier transform of a function $\mathcal{F}$ which is related to the sea surface's geometry characteristics,

$$\mathcal{F}(\mathbf{r}) = e^{-\frac{1}{2}Q_z^2\mathcal{D}(\mathbf{r})}. \tag{31}$$

So, the correct estimation of the NRCS is linked to the estimation accuracy of the function $\mathcal{F}$ and the application of the SDM. In what follows, the numerical results of key generated surface characteristics –and the function $\mathcal{F}$ in particular– are presented to assess the advantages of the SDM.

4 Generated Surface Characteristics

It is necessary to analyze the characteristics of the generated surfaces with the SDM and compare to those obtained with conventional methods. First, the impact of the interpolation process (for LF sea surface generation) on sea surface height spectrum is investigated. Secondly, the generated surface characteristics resulting from the combination techniques (for HF sea surface generation) introduced in subsection 2.3 are studied. Thirdly, the height spectrum and the height structure function are computed. At last, the key function $\mathcal{F}$ from (31) is calculated.

For a sake of clarity, this study is conducted for 2D problems but the results can be extended to 3D problems.

4.1 Interpolation Techniques

One scenario is proposed here and the parameters are listed in Table 2. In (19) the parameter P is defined as $P \times L = L_0$ with L the length of the elementary HF sea surface and L_0 both the length of the LF sea surface and the one of the total two-scales composite surface H (18). Then, by considering the number of samples M and the sampling interval ΔX as invariant parameters, the LF sea surface parameters are M samples and a sampling interval of $P\Delta X$. So, P is the interpolation parameter, moving from the sampling interval $P\Delta X$ to ΔX. Moreover, regarding the elementary HF sea surface parameters, M samples and a sampling interval of ΔX are used, implying the combination of P elementary surfaces to reach the length L_0.

Table 2: Simulation Parameters

Frequency f	10 GHz
Radar wavelength λ_0	0.03 m
Number of samples M	2^{13}
Sampling interval ΔX	$\lambda_0/10$
Wind speed u_{10}	8 m/s

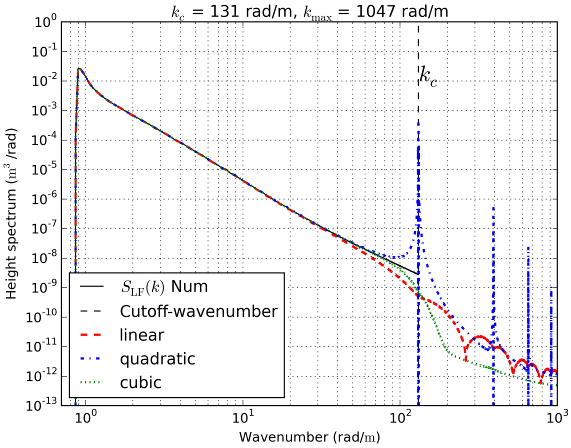

Figure 7: Isotropic part of the sea surface height spectrum S_{LF} from the model of Elfouhaily et al. [*Elfouhaily et al.*, 1997]. Wind speed is $u_{10} = 8$ m/s. The numerical spectrum S_{LF} –with sea surface generation– is presented. The cutoff-wavenumber before the interpolation process $k_c = 131$ rad/m is also displayed. Three interpolation techniques are illustrated, linear, quadratic and cubic.

Figure 7 illustrates the isotropic part of the sea surface height spectrum from the model of Elfouhaily et al. [*Elfouhaily et al.*, 1997]. Three interpolation techniques are studied: linear, quadratic and cubic. The full sea surface height spectrum is obtained by numerical computation ($S_{\mathrm{LF}}(k)$ Num) with a Monte Carlo method by generating 500 sea surfaces and computing the mean sea surface height spectrum. Figure 7 shows that the interpolated surface creates higher frequency harmonics than the original surface. Also, it can be seen that the quadratic interpolation presents over-occurred harmonics which can severely disturb the NRCS, especially by using the Small Perturbation Method (SPM), which is directly proportional to high-frequencies sea surface height spectrum. Besides, linear and cubic interpolations seem to be relevant techniques to upgrade the sampling intervals of a given sea surface, creating low energy high frequency components. So, the linear interpolation is the best choice which, in addition, optimizes computation time and memory resources.

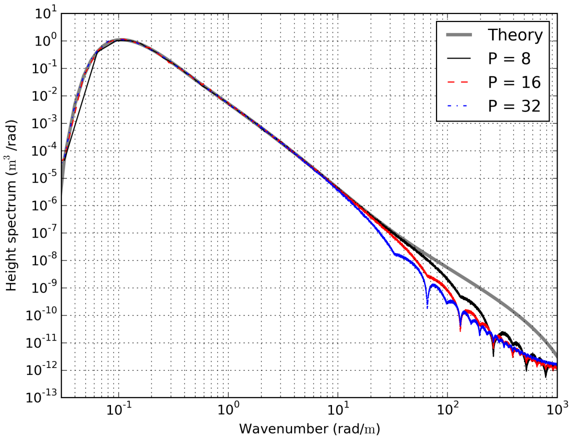

Figure 8: Isotropic part of the interpolated sea surface h_{LF} height spectrum from the model of Elfouhaily et al. [*Elfouhaily et al.*, 1997]. Wind speed is $u_{10} = 8$ m/s. Three interpolation parameters are presented, $P = \{8; 16; 32\}$, the interpolation method is linear. The isotropic part of the sea surface height spectrum from the model of Elfouhaily is also displayed (Theory).

Figure 8 plots the isotropic part of the interpolated sea surface height spectrum. The linear interpolation method is considered here. Three values of the interpolation parameter are studied: 8, 16 and 32. The results show a qualitatively-low impact of the interpolation parameter , this has to be discussed further after adding the reconstructed HF sea surface. Indeed, the isotropic part of the interpolated sea surface height spectrum remains less energetic than the isotropic part of the full sea surface height spectrum on the interpolation interval; this does not matter here since this part of the spectrum will be dominated by the HF part leading to the vanishing of the interpolation effect. Besides, the greater the interpolation parameter P, the earlier the oscillations occur in the sea surface height spectrum. This phenomenon is explained by the chosen sampling interval. Indeed, before the interpolation process, the cutoff-wavenumber is $k_c = \pi/(P\Delta X)$, so, the greater the interpolation parameter P, the smaller k_c and therewith, the earlier the oscillations occur. Therefore, an interpolation process –especially when linear– is efficient to reduce the sampling interval to having almost no added cost.

4.2 Combination Techniques

The scenario in this section is similar to the one in subsection 4.1, Table 2 but here, the HF part is considered rather than the LF one. Elementary HF sea surfaces are now combined with one of the techniques presented in subsection 2.3. Before the combination process, the elementary HF surface length L is $M \times \Delta X$ and after combination, the reconstructed HF sea surface length will be $P \times L$ with P the combination parameter. Thus, the minimum wavenumber before combination is $k_{\min} = 2\pi/L$.

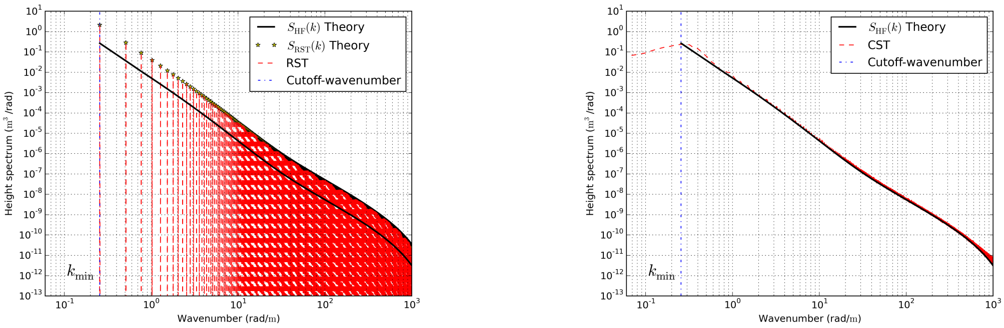

(a) Repeated Surfaces Technique

(b) Combined Surfaces Technique

Figure 9: Isotropic part of the high-frequency sea surface height spectrum S_{HF} from the model of Elfouhaily et al. [*Elfouhaily et al.*, 1997]. Wind speed is $u_{10} = 8$ m/s. The minimum wavenumber before the combination process k_{min} is also displayed. The isotropic part of the combined sea surfaces $h_{\mathrm{HF,T}}$ height spectrum from the two combination techniques introduced in subsection 2.3 are also illustrated; RST (9a) and CST (9b).

Figure 9 plots the isotropic part of the high-frequency sea surface height spectrum. This spectrum is compared to those obtained using combination techniques. Figure 9a illustrates the RST spectrum, the theoretical spectrum of RST previously derived in (15) is also displayed and is in accordance with the numerical one. The RST slightly overestimates the harmonics within the spectrum. Seemingly, the RST spectrum is "noisy". In fact, regarding (15), the function modulating the high-frequency sea surface height spectrum operates as a sampling function (such as the Dirac delta function) and so, some harmonics within the spectrum are periodically conserved while others are forced to a residual value, like a Dirac comb function. This process ensures a good conservation of the energy within the spectrum. Despite the apparition of harmonics at wavenumbers smaller than k_{min}, the CST seems to get the best accuracy by ensuring continuity and avoiding overestimated harmonics (Figure 9b). Moreover, the SDM height's mean square value ($\sigma^2_{\mathrm{HF,\ X}}$ with X the combination technique) is in accordance with the conventional one (σ^2_{HF}). Indeed, $\sigma^2_{\mathrm{HF}} = 0.084$ m^2, $\sigma^2_{\mathrm{HF,\ RST}} = 0.086$ m^2 and $\sigma^2_{\mathrm{HF,\ CST}} = 0.083$ m^2.

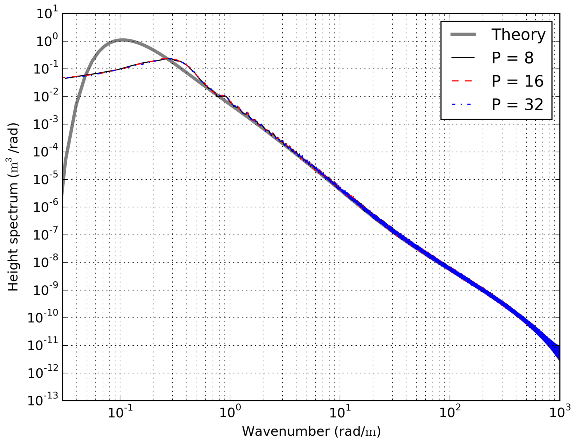

Figure 10: Isotropic part of the height spectrum of the combined sea surfaces $h_{\mathrm{HF,T}}$ from the model of Elfouhaily et al. [*Elfouhaily et al.*, 1997]. Wind speed is $u_{10} = 8$ m/s. The inspected combination technique is the CST. Three parameters are shown; 8 ($k_{\min} = 0.032$ rad/m), 16 ($k_{\min} = 0.016$ rad/m) and 32 ($k_{\min} = 0.008$ rad/m). The isotropic part of the sea surface height spectrum from the model of Elfouhaily is also displayed (Theory).

Figure 10 plots the height spectrum of the combined sea surfaces by using the CST. Whatever the parameter P is (between 8 and 32), the height spectrum is qualitatively similar.

4.3 Height Spectrum and Height Structure Function

The SDM is applied to create an $M \times P$-samples composite two-scales sea surface with a sampling interval ΔX. Firstly, one sea surface with M samples and a sampling interval $P \times \Delta X$ is generated and then linearly interpolated to get a new sampling interval ΔX, this is the LF sea surface. Secondly, one sea surface with M samples and a sampling interval ΔX is generated to perform RST ($2P$ realizations are necessary for CST) and therefore, to create a combined sea surface with $M \times P$ samples and a sampling interval ΔX, this is the reconstructed HF sea surface. Then, these two surfaces are added to generate the composite two-scales surface. Notice that, to avoid spectral redundancy between the two spectra used to generate these two surfaces, harmonics in the interval I are forced to 0 in the first spectrum –that is the LF part– with

$$I = \left[\frac{2\pi}{M\Delta X}, \frac{\pi}{P\Delta X} \right]. \tag{32}$$

The frequency is 10 GHz, $M = 2^{13}$ samples, $\Delta X = \lambda_0/10$ with λ_0 the wavelength, $P = 8$ and the wind speed u_{10} is 8 m/s. This generation is repeated in a Monte Carlo process by generating 500 composite two-scales sea surfaces.

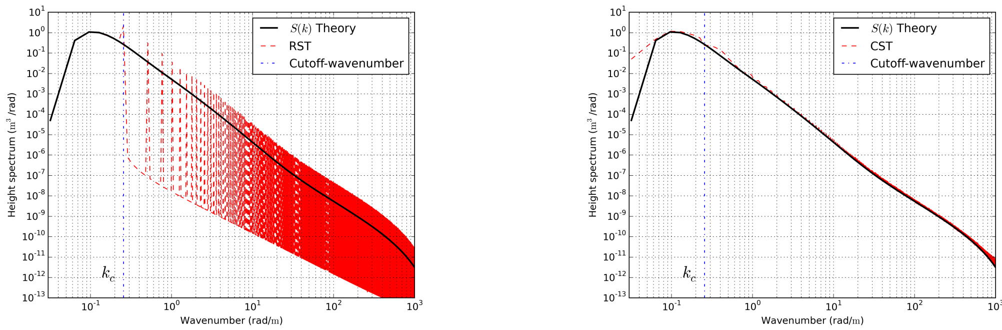

(a) Repeated Surfaces Technique

(b) Combined Surfaces Technique

Figure 11: Isotropic part of the full sea surface height spectrum $S(k)$ from the model of Elfouhaily et al. [*Elfouhaily et al.*, 1997]. Wind speed is $u_{10} = 8$ m/s. The isotropic part of the composite two-scales sea surface H height spectrum from the two combination techniques introduced in subsection 2.3 are also illustrated; RST (11a) and CST (11b) with $P = 8$.

Figure 11 plots the isotropic part of sea surface height spectrum. This spectrum is compared to those obtained using the SDM. Once again, harmonics at wavenumbers smaller than $k_c = 2\pi/(M\Delta X)$ are greater than their theoretical counterparts in CST, Figure 11b. Indeed, this technique is based on the combination of independent surfaces. Figure 11a illustrates the RST. As previously depicted in Figure 9, the RST overestimates the harmonics within the spectrum. Finally, the CST again gets the best accuracy by ensuring continuity and avoiding overestimated harmonics. To complete the spectral investigation of SDM, a spatial analysis of the height structure function introduced in (30) is interesting. Indeed, this quantity leads to the NRCS estimation by using SSA1 (29).

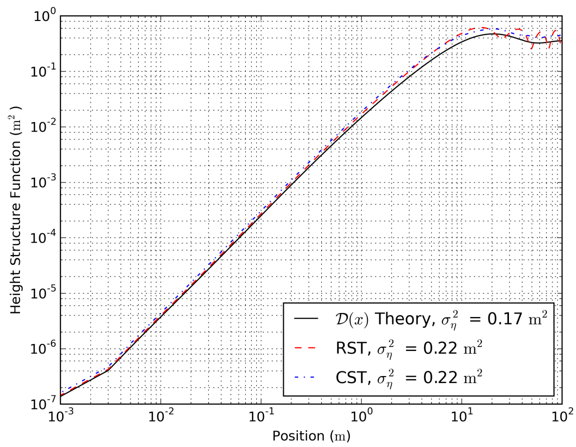

Figure 12: Height structure function $\mathcal{D}$ from the model of Elfouhaily et al. [*Elfouhaily et al.*, 1997]. Wind speed is $u_{10} = 8$ m/s. The theoretical height structure function $\mathcal{D}$ is plotted in solid black line. The composite two-scales sea surface H height structure function from the two combination techniques (subsection 2.3) are illustrated in dashed-red and discontinuous-blue line; RST and CST, respectively, with $P = 8$.

Figure 12 plots the theoretical height structure function $\mathcal{D}(x)$ estimated from (30). This height structure function is compared to the two obtained with SDM. The RST produces oscillations within the height structure function. This phenomenon is induced by the repetition process and so, by the correlation renewal between one surface elevation point and its copy, located every $M \times \Delta X$ meters. The CST height structure function is qualitatively in accordance with the theoretical one. Furthermore, the overestimation of the height mean square value σ_η^2 is induced by the interpolation process which creates –as previously described in subsection 4.1– high-frequency harmonics in the spectrum. Still, this overestimation remains quantitatively low.

4.4 From sea surface characteristics to NRCS

The right description of the function $\mathcal{F}$ defined in (31) is a crucial step into the NRCS computation. Indeed, as previously described, this function is one of the key-parameter in the analytical expression of the NRCS with SSA1 (29). Despite a modified description of the sea surface height spectrum by SDM, by ensuring a non-impact of combination techniques on the function $\mathcal{F}$, SDM becomes an advantageous way to compute the NRCS from sea surfaces.

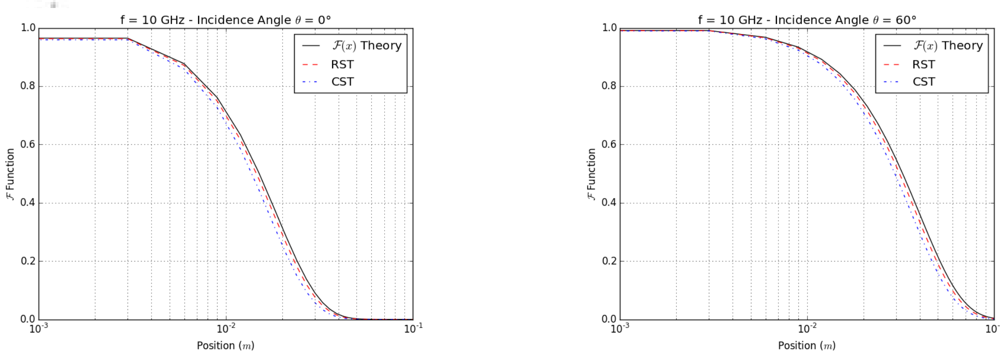

(a) Incidence Angle 0°

(b) Incidence Angle 60°

Figure 13: $\mathcal{F}$ function from the model of Elfouhaily et al. [*Elfouhaily et al.*, 1997]. Wind speed is $u_{10} = 8$ m/s for a frequency $f = 10$ GHz. The theoretical $\mathcal{F}$ function is plotted (Theory). The $\mathcal{F}$ functions from the composite two-scales sea surface H with the two combination techniques (subsection 2.3) are illustrated; RST and CST.

Figure 13 plots the theoretical $\mathcal{F}$ function. Those computed by using SDM and the two different combination techniques, RST and CST, are also displayed. Two incidence angles are considered here, $\theta = 0°$, which is located in the Geometrical Optics domain, and $\theta = 60°$ in the Bragg scattering domain. SDM is in agreement with the theory independently of the combination technique used. Therefore, according to (31), the SDM should not disturb the NRCS estimation. This statement is assessed hereafter.

5 Sea Surface Monostatic NRCS

A two-dimensional problem is considered to compute the sea surface NRCS. The same parameters introduced in Table 2 are chosen and the SDM parameter P (that is either the interpolation parameter or the combination one) is 8. The sea surface NRCS is computed with a monostatic configuration and the sea dielectric permittivity ε is

$53.2 + j37.8$. To obtain this NRCS, a hundred of sea surfaces are generated. Thus, the surface length is $M \times P \times \Delta X \approx 196$ m and the gravity waves are correctly taken into account in the sea surface height spectrum (25). For this scenario, the impact induced by the combination technique –and therefore the SDM– on the sea surface NRCS is studied.

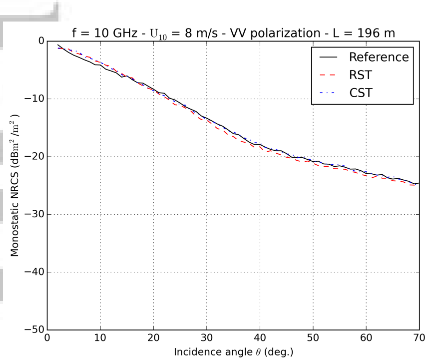

(a) Incoherent monostatic NRCS versus the incidence angle, VV polarization

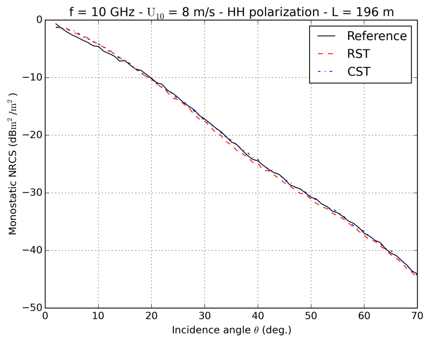

(b) Incoherent monostatic NRCS versus the incidence angle, HH polarization

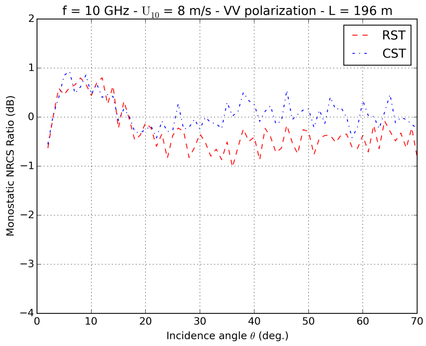

(c) Incoherent monostatic NRCS ratio versus the incidence angle, VV polarization

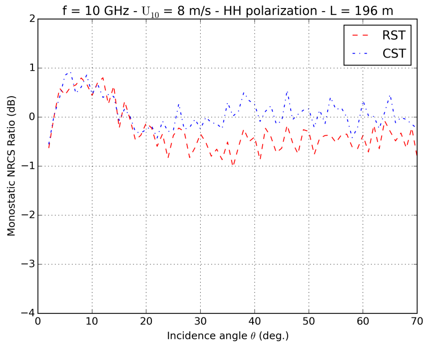

(d) Incoherent monostatic NRCS ratio versus the incidence angle, HH polarization

Figure 14: The wind speed is 8 m/s for a frequency $f = 10$ GHz in VV and HH polarizations. Comparison of the NRCS from conventional sea surface generation and the NRCS from SDM, considering the two different combination techniques. 100 surfaces of length $L = 196$ m were generated.

Figures 14a and 14b plot the incoherent monostatic NRCS versus the incidence angle from a conventional sea surface generation –spectral method introduced in subsection 2.1– and from SDM with either RST or CST. The ratios between RST / CST and the reference are also shown in Figures 14c and 14d. One can see that the SDM and any of the suggested combination techniques do not quantitatively disturb the NRCS estimation, both in VV and HH polarizations. For RST, the maximal error is ± 1 dB and for CST, the error is about 0 dB after the incidence angle 15° and remains inferior to ± 1 dB along the incidence angle track. The error function is similar for both polarizations. Indeed, only the sea surface generation process is modified and this does not impact on the polarization term within SSA1 (26). Two more scenarios are investigated in Appendix B: again, it is observed that the SDM and any of the suggested combination techniques do not quantitatively disturb the NRCS in VV and HH polarizations. Thus, SDM with RST is an efficient means to perform numerical computation of the sea surface NRCS. Then, the effect of the parameter P is investigated. Three values are chosen, $P = \{8, 16, 32\}$ corresponding to the memory consumption ratios $\{0.031, 0.008, 0.002\}$ for RST (Table 1). To keep the same sea surface length, the number of samples M is modified in consequence and the sampling interval is kept constant, $\Delta X = \lambda_0/10$, as previously stated. The two polarizations VV and HH are studied.

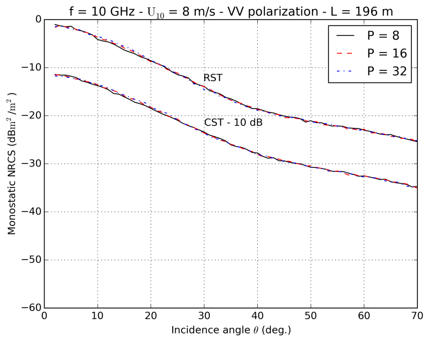

(a) Incoherent monostatic NRCS versus the incidence angle, VV polarization, RST and CST - 10 dB

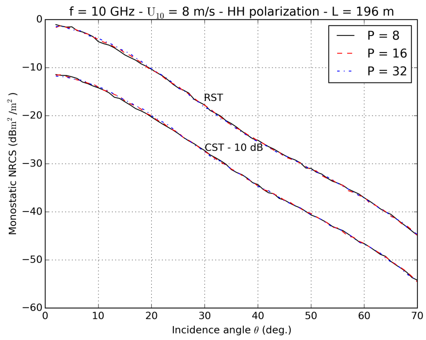

(b) Incoherent monostatic NRCS versus the incidence angle, HH polarization, RST and CST - 10 dB

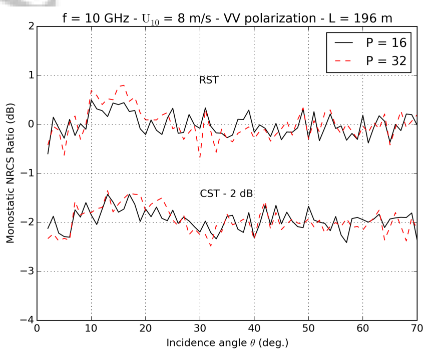

(c) Incoherent monostatic NRCS ratio versus the incidence angle, VV polarization, RST and CST - 2 dB

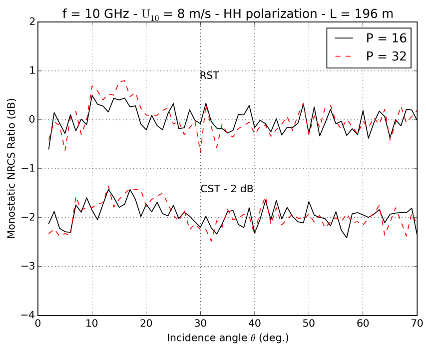

(d) Incoherent monostatic NRCS ratio versus the incidence angle, HH polarization, RST and CST - 2 dB

Figure 15: The wind speed is 8 m/s for a frequency $f = 10$ GHz in VV and HH polarizations. Comparison of the NRCS with different P parameters and considering the two combination techniques. 100 surfaces of length $L = 196$ m were generated. CST - X dB stands for an offset of X dB to improve the discrimination between the two techniques.

Figures 15a and 15b plot the incoherent monostatic NRCS in VV or HH polarization versus the incidence angle from SDM with either RST or CST and by applying different P parameters. The two combination techniques are distinguished by an offset (-10 dB for CST). The results show a same trend for VV or HH polarizations, the tested P values show no impact on the result. This observation is confirmed by Figures 15c and 15d. Indeed, the NRCS ratio between $P = \{16, 32\}$ and $P = 8$ is inferior to ± 1 dB along the incidence angle track, and so, whatever the investigated combination technique. Again, the two combination techniques are distinguished by an offset (-2

dB for CST). Like in Figures 14c and 14d, these error functions are similar; the sea surface generation process does not interfere with the polarization term in SSA1 (26).

From the results presented in this paper, it can be finally concluded that SDM can be used to compute the NRCS of an ocean surface.

6 Summary and Outlooks

Sea surface wave generation is a highly resource-demanding process to achieve accurate NRCS at microwave frequencies. Indeed, large sea surface areas and high resolution are required. In this context, the Spectral Decomposition Method (SDM) is a useful tool to make the sea surface wave generation faster and less memory demanding. Interpolation and combination techniques which complete the SDM have been presented. Three kinds of interpolation, linear, quadratic and cubic have been considered as well as two combination techniques, the Repeated Surfaces Technique (RST) and the Combined Surfaces Technique (CST). A study of the computational complexity of SDM has shown that the SDM reduces the complexity by a factor 10 to 200, depending on the chosen combination technique. Similarly, the memory requirement is shown to be drastically reduced by using SDM rather than the conventional spectral method, the reduction ratio is roughly 10^{-2} to 10^{-3}. The SDM and these interpolation and combination techniques have been studied with regards to the characteristics of the generated sea surface geometry as well as with regards to the sea surface monostatic NRCS. The linear interpolation method appeared to be the best choice as it is the quickest interpolation process while presenting only weak distortions of the sea surface height spectrum (a crucial characteristic since its inverse Fourier transform is linked to the sea surface NRCS computed with SSA1). Using RST leads to a sea surface height spectrum being the conventional spectrum modulated by a periodic function. This behavior –never previously highlighted in the literature– has been analytically derived and numerically validated. The CST leads to a sea surface height spectrum close to the conventional one, excepting a few low frequency components. In spite of these differences, the height structure function of RST and CST are close to the one obtained with the conventional spectral method. As a consequence, the sea surface monostatic NRCS computed from the SDM with either the RST or the CST is in good agreement with the one computed from a conventional sea surface generation. Therefore, the SDM is demonstrated to be valid from near nadir to moderate observation angles. This approach is analytically formalized –both in spatial and frequency domains for RST– and tested for a subdivision in two spectra according to the sea surface geometry characteristics and the monostatic NRCS.

It can therefore be concluded that the SDM is a useful tool to accelerate the radar backscattering computation from large sea surfaces. In future work, it should be coupled with a two-scale electromagnetic model to further speed up the simulation. Moreover, the spectral decomposition method could be used to simulate sea surface waves with range variations of characteristics (wind speed in particular) and then to compute composite sea surface waves, closer to the real weather conditions.

A: RST Sea Surface Height Spectrum

From (9),

$$h_{\mathrm{HF,T}}(x) = h_{\mathrm{HF}}(x) * \sum_{a=0}^{A-1} \delta(x - aL) = \sum_{a=0}^{A-1} h_{\mathrm{HF}}(x - aL), \tag{A.1}$$

with h_{HF} the A-times-repeated surface, L its length, $h_{\mathrm{HF,T}}$ the reconstructed sea surface of length $A \times L$ and δ the Dirac delta function. Then, the height autocorrelation function $W_{\mathrm{HF,RST}}$ corresponding to the RST is expressed as

$$\begin{aligned} W_{\mathrm{HF,RST}}(r) &= \frac{1}{A}\sum_{a=0}^{A-1}\sum_{b=0}^{A-1}\langle h_{\mathrm{HF}}(x_1-aL)h^*_{\mathrm{HF}}(x_1+r-bL)\rangle \\ &= \frac{1}{A}\sum_{a=0}^{A-1}\sum_{b=0}^{A-1}\langle h_{\mathrm{HF}}(\alpha_a)h^*_{\mathrm{HF}}(\alpha_a+r+(a-b)L)\rangle \\ &= \frac{1}{A}\sum_{a=0}^{A-1}\sum_{b=0}^{A-1} W_{\mathrm{HF}}(r+(a-b)L), \end{aligned} \tag{A.2}$$

with W_{HF} the theoretical height autocorrelation function, x_1 an abscissa and $\alpha_a = x_1 - aL$. Therefore, by taking the Fourier transform of the height autocorrelation function, one can get

$$S_{\mathrm{HF,RST}}(k) = \frac{S_{\mathrm{HF}}(k)}{A}\sum_{a=0}^{A-1}\sum_{b=0}^{A-1}\exp[jk(a-b)L]. \tag{A.3}$$

Furthermore,

$$\sum_{a=0}^{A-1}\sum_{b=0}^{A-1}\exp[jk(a-b)L] = \left[\sum_{a=0}^{A-1}\exp(jkaL)\right]\left[\sum_{b=0}^{A-1}\exp(jkbL)\right]^*. \tag{A.4}$$

This expression can be simplified by using formulas from geometric series to finally obtain

$$S_{\mathrm{HF,RST}}(k) = \frac{1}{A}\frac{\sin^2(\frac{kAL}{2})}{\sin^2(\frac{kL}{2})}S_{\mathrm{HF}}(k), \tag{A.5}$$

with $S_{\mathrm{HF}}(k)$ the theoretical sea height spectrum. That is the response of a uniform linear array of phased antennas with S_{HF} the elementary antenna.

B: Sea Surface Monostatic NRCS, Additionnal Scenarios

Figure B.1 plots the incoherent monostatic NRCS versus the incidence angle from a conventional sea surface generation –spectral method introduced in subsection 2.1– and from SDM with either RST or CST for two scenarios. These scenarios are: a radar frequency $f = 5$ GHz and a wind speed $u_{10} = 8$ m/s for the first and $f = 10$ GHz, $u_{10} = 5$ m/s for the second. As previously observed in section 5, the SDM and any of the suggested combination techniques do not quantitatively disturb the NRCS, both in VV and HH polarizations.

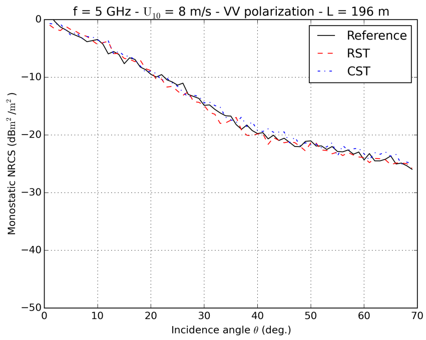

(a) Wind speed of 8 m/s, frequency $f = 5$ GHz, VV polarization

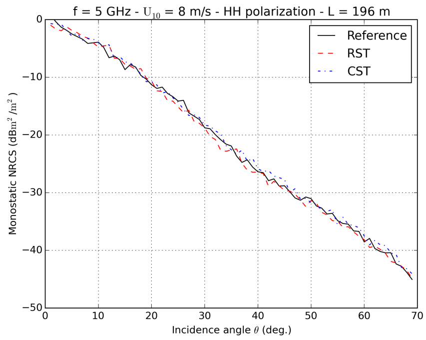

(b) Wind speed of 8 m/s, frequency $f = 5$ GHz, HH polarization

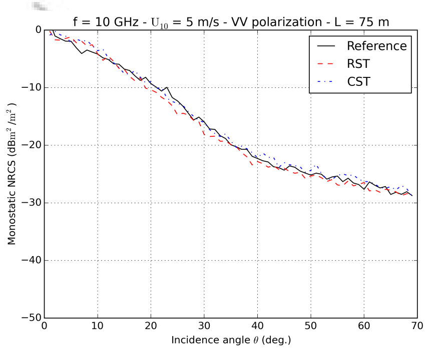

(c) Wind speed of 5 m/s, frequency $f = 10$ GHz, VV polarization

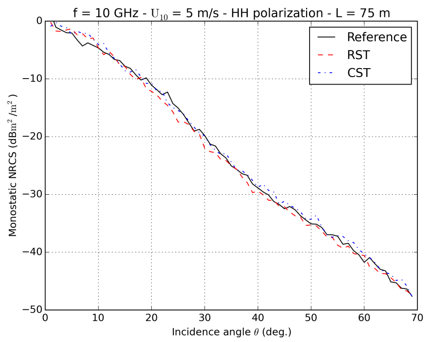

(d) Wind speed of 5 m/s, frequency $f = 10$ GHz, HH polarization

Figure B.1: Incoherent monostatic NRCS versus the incidence angle. Comparison of the NRCS from conventional sea surface generation and the NRCS from SDM, considering the two different combination techniques. 100 surfaces were generated.

Acknowledgments

The authors would like to thank the Total company for funding and especially Veronique Miegebielle and Dominique Dubucq for supporting this work. No specific data were used to produce this manuscript.

References

Bourlier, C. (2018), Upwind Downwind Asymmetry of the Sea Backscattering Normalized Radar Cross Section Versus the Skewness Function, *IEEE Transactions on Geoscience and Remote Sensing*, *56*(1), 17–24.

Bourlier, C., and N. Pinel (2009), Numerical implementation of local unified models for backscattering from random rough sea surfaces, *Waves in Random and Complex Media*, *19*(3), 455–479, doi:10.1080/17455030902988931.

Bourlier, C., N. Déchamps, and G. Berginc (2005), Comparison of asymptotic backscattering models (SSA, WCA, and LCA) from one dimensional Gaussian ocean-like surfaces, *IEEE Transactions on Antennas and Propagation*, *53*(5), 1640–1652, doi:10.1109/TAP.2005.846800.

Bourlier, C., N. Pinel, and G. Kubicke (2013), *Method of Moments for 2D Scattering Problems: Basic Concepts and Applications*, John Wiley & Sons, Inc., Hoboken, USA.

Elfouhaily, T. M., B. Chapron, K. Katsaros, and D. Vandemark (1997), A unified directional spectrum for long and short wind-driven waves, *Journal of Geophysical Research: Oceans*, *102*(C7), 15,781–15,796, doi:10.1029/97JC00467.

Jeannin, N., L. Féral, H. Sauvageot, L. Castanet, and F. Lacoste (2012), A Large-Scale Space-Time Stochastic Simulation Tool of Rain Attenuation for the Design and Optimization of Adaptive Satellite Communication Systems Operating between 10 and 50 GHz, *International Journal of Antennas and Propagation*, *2012*, doi:10.1155/2012/749829.

Jiang, W., M. Zhang, P.-B. Wei, and D. Nie (2015), Spectral Decomposition Modeling Method and Its Application to EM Scattering Calculation of Large Rough Surface With SSA Method, *IEEE Journal of Selected Topics in Applied Earth Observations and Remote Sensing*, *8*(4), 1848–1854.

Jiang, W., M. Zhang, Y. Zhao, and D. Nie (2016), EM scattering calculation of large sea surface with SSA method at S , X , Ku , and K bands, *Waves in Random and Complex Media*, *5030*, doi:10.1080/17455030.2016.1213463.

McDaniel, S. (2001), Small-slope predictions of microwave backscatter from the sea surface, *Waves in Random Media*, *11*(3), 343–360.

Pinel, N., G. Monnier, J. Houssay, and A. Becquerel (2014), Fast simulation of a moving sea surface remotely sensed by radar, in *International Radar Conference*, IEEE.

Tessendorf, J. (2001), Simulating Ocean Water, *Environment*, *2*, 1–19, doi:10.1016/j.chemosphere.2006.11.013.

Tsang, L., J. Au Kong, K.-H. Ding, and C. O. Ao (2002), *Scattering of Electromagnetic Waves: Numerical Simulations*, John Wiley & Sons, Inc., doi:10.1002/0471224308.

Voronovich, A. G. (1986), Small-slope approximation in wave scattering by rough surfaces, *Journal of Experimental and Theoretical Physics*, *62*, 65–70.

Voronovich, A. G., and V. U. Zavorotny (2001), Theoretical model for scattering of radar signals in Ku- and C-bands from a rough sea surface with breaking waves, *Waves in Random Media*, *11*(3), 247–270, doi:10.1080/13616670109409784.

Ghaleb, Antoine, Even, Stéphanie, Garello, René, Chapron, Bertrand, Pinel, Nicolas, and De Beaucoudrey, Nicole (2010), Modeling and simulation of sea surface radar observations, *Simulation.*

Franceschetti, Giorgio, Migliaccio, Maurizio, and Riccio, Daniele (1998), On Ocean SAR Raw Signal Simulation, *IEEE Transactions on Geoscience and Remote Sensing*, *36*(1), 84–100.

Franceschetti, Giorgio, Iodice, Antonio, Riccio, Daniele, Ruello, Giuseppe, and Siviero, Roberta (2002), SAR Raw Signal Simulation of Oil Slicks in Ocean Environments, *IEEE Transactions on Geoscience and Remote Sensing*, *40*(9), 1935–1949.

Wei, Peng-Bo, Min, Zhang, Nie, Ding and Jiao, Yong-Chang (2018), Statistical realisation of CWMFSM for scattering simulation of space-time varying sea surface, *International Journal of Remote Sensing*, 1–14.